7-7-2012

Distribution of microcrack lengths in bone in vivo and in vitro.

Gerardo Presbitero
Trinity College Dublin

Fergal O'Brien
Royal College of Surgeons in Ireland, fjobrien@rcsi.ie

T Clive Lee
Royal College of Surgeons in Ireland

David Taylor
Trinity College Dublin

Citation

Presbitero G, O'Brien F, Lee TC, Taylor D. Distribution of microcrack lengths in bone in vivo and in vitro. Journal of Theoretical Biology. 2012;304:164-171.

DISTRIBUTION OF MICROCRACK LENGTHS IN BONE *IN VIVO* AND *IN VITRO*

Gerardo Presbitero[a,*], Fergal O'Brien[b], T. Clive Lee[b] and David Taylor[a]

[a]*Trinity Centre for Bioengineering, Trinity College Dublin, Dublin 2, Ireland*
[b]*Department of Anatomy, Royal College of Surgeons in Ireland, St. Stephens Green, Dublin 2, Ireland*

*Corresponding author: Trinity Centre for Bioengineering, Trinity College Dublin, College Green, Dublin 2, Ireland. Tel.: +353-1-8964214; fax: +3531 679 5554. *Email address*: presbitg@tcd.ie

fjobrien@rcsi.ie (F. O´Brien); tclee@rcsi.ie (T.C. Lee); dtaylor@tcd.ie (D. Taylor)

ABSTRACT
It is well known that bone contains small cracks; in vivo these microcracks are constantly growing and being repaired. Too rapid crack growth leads to stress fractures or fragility fractures. In vitro, changes occur in this population of microcracks when subjected to cyclic loading up to and including failure.
Normally, the only parameters reported from such investigations are the number density of cracks and their average length. In the present work we examined the microcrack population in more detail. We analysed ten different sets of experimental data including in vivo and in vitro microcracks, plus two theoretical simulations. We showed for the first time that the distribution of crack lengths can be described using the two-parameter Weibull equation. The values of the two constants in the equation varied depending on bone type/species and showed consistent trends during in vitro testing. This is the most detailed study to be conducted on microcrack populations in bone; the results will be useful in future studies including the development of theoretical models and computer simulations of bone damage and failure.

* Corresponding author: Tel.: +353-1-8964214, +353 1 896 1383; fax: +3531 679 5554
Email address: presbitg@tcd.ie

INTRODUCTION

Stress fractures and fragility fractures in bone are a major cause for concern, especially in relatively active individuals and those whose bone strength is compromised. For example, military recruits suffer high rates of stress fractures during training [1] and 5-15% of all injuries to runners are caused by stress fractures [2]. Fragility fractures occur predominantly in people suffering from osteoporosis: in the UK 200,000 such fractures occur each year and worldwide fracture rates are predicted to rise to 6 million within 50 years. Between 2.5% and 12% of people aged 65 or over will suffer a fracture by falling, and a third of women and one in 12 men over 50 years will suffer an osteoporosis-related fracture at some time in their life [3].

Stress fractures occur as a result of fatigue mechanisms caused by the action of cyclic stress, which leads to the formation and growth of microcracks, especially when bone is loaded in compression, which is the predominant loading mode *in vivo* [4]. Bone is a material in which cracks readily form, but find it difficult to grow, and they tend to remain small and follow the direction of easy growth, parallel to lamellae and osteons, which is approximately parallel to the longitudinal axis in the long bones [5]. Microcracks were first observed by Frost [6, 7] who correctly hypothesized that one of the functions of bone remodeling is to repair the tissue by removing these cracks. Since then many workers have observed and measured microcracks; the great majority of these studies involved detecting cracks by microscopic examination of transverse sections cut from bones *ex vivo* or from test samples after *in vitro* cyclic loading. The parameters normally presented in publications are the number density, expressed as the number of cracks per unit area (rather than the true density which would be per unit volume) and the average crack length. Another parameter, the surface crack density, records the total crack length per unit area, this being simply the product of the other two parameters [8-11].

Some workers have attempted to observe and record the rates of growth of individual cracks during cyclic loading [12,13], though to date this kind of work has received little attention. There have also been some attempts to develop theoretical models and computer simulations of their growth [14]. The threshold for crack formation and the mechanisms responsible for initiating microcracks are still poorly understood [1], and this is a major limitation in the development of theoretical models.

The normal description of bone damage in terms of the two parameters described above – crack density and average crack length – omits information about the distribution of crack lengths within the sample observed. We reasoned that this extra information might be useful in understanding the development of damage and eventual failure and in formulating theoretical models and simulations. We hypothesised that the distribution of crack lengths could be described by some standard form such as a Weibull or Gaussian distribution. If so, since this distribution can be fully described by a small number of constants, we hypothesised that the values of these parameters, which essentially characterise the state of damage in the material, would vary in a systematic way with parameters such as the type of bone, the type of animal and the loading conditions, whether *in vivo* or *in vitro*, such as the applied stress range and number of cycles. The aims of the present work were to investigate these hypotheses using data from our own experimental work and that of others.

MATERIALS AND METHODS

We collected data on the lengths of individual microcracks, using results obtained previously from our research group, consisting of *in vivo* ovine bone data [15], bovine bone data from work published previously [16] and bovine bone data obtained from new tests as described below. We also contacted other researchers, who had published work in this field [17, 18], who kindly agreed to provide us with their original crack length measurements which had not appeared in their publications. These studies recorded crack lengths either from bones which had been subjected only to *in vivo* loadings or else bones (or test specimens made from bones) which were subjected to additional cyclic loading *in vitro*, at some specified range of stress or strain for a specified number of cycles.

Table 1 summarizes the test conditions in each case. The definition of microcrack length is the distance between the two tips of the crack as seen on transverse sections. The range of stress or strain is defined as the difference between the maximum and minimum values in the cycle imposed.

Table 1: *Summary of data sources*

These data cover a useful range of loading conditions, from *in vivo* loading, which typically includes strains up to 2000-3000με [19], equivalent to a stress range of approximately 40-50MPa, to *in vitro* testing at higher stress ranges up to 80MPa. Results obtained by [20] reported slightly less than 2000 με when measuring tibial shafts of soldiers during intensive training regimes. The highest strains registered *in vivo* are the results obtained by [21], measuring compressive strains in racehorses ranging from 4400 to 5670 με. In addition one should remember that *in vivo*, microdamage is being continuously repaired, whilst *in vitro* this is not the case, so there could be differences in the data for *in vitro* loading within the *in vivo* range, as in the tests of Burr *et al* 1998 at 2700με.

Experimental Tests

New test data were obtained for bovine bone at a stress range of 70MPa. In this work we used the same protocol as described previously [16], the only difference being the stress level. Ten cylindrical samples of bovine bone were obtained using a coring device, the longitudinal axis of the sample corresponding to the bone's axis. The diameter of the sample was reduced in a central portion and the ends were inserted in metal caps to facilitate attachment to a servo-hydraulic testing machine. Ranges for physiological frequencies are given between 0.5 and 3 Hz, in the present work cyclic loading was carried out in compression at a frequency of 3Hz; the ratio of the minimum stress to the maximum stress was 0.1. Tests performed by researchers such as the ones published by Burr *et al*. [17], used a one single dye, for which it was necessary to test two separate groups of bones: one to study microdamage developed *in vivo*, the other to study microdamage developed under external fatigue loads. The tests performed in the current work used three different coloured dyes, to label microcracks in the same specimens at three stages: the start of the test (i.e. *in vivo* cracks); after 50,000 cycles and after fracture or one million cycles, whichever happened first. The reason for selecting 50,000 cycles for the second dye was to detect microcracks which formed after a relatively small number of cycles, compared to the number of cycles to failure, since it has previously been observed that significant numbers of cracks form in this early stage [16].

The dimensions of the samples used in these tests (gauge length, reduced diameter, radius of curvature at transition region, grip region length) are shown in Figure 1.

Figure 1: *Details of specimens and their orientation in the testing machine. All dimensions in millimetres.*

Simulation of microcrack distribution

In addition to obtaining experimental data on microcrack length distributions, we also attempted to simulate this data, in two different ways. In both cases the underlying assumption was that microcracks initiate in the so-called interstitial bone (i.e. in those regions of bone which lie outside the osteons) and that cracks tend to stop growing when their tips reach the cement lines surrounding osteons. Figure 2 illustrates cement lines stopping the growth of a microcrack (a) [22]; and a crack passing close to an osteon tending to be attracted towards the cement line (b), in a sample of the bovine bone tests from the current work.

Given sufficient time and/or stress, these cracks may continue to elongate, but our previous work [23, 24] and that of others [25] has shown that 80-90% of all cracks become dormant at an early stage. Thus we reasoned that an approximate simulation of the distribution of microcrack lengths, at least for the great majority of cracks, might be obtained simply by measuring the distance between adjacent cement lines.

Figure 2(a): *Microcrack growth stopped by its tips when encountering the cement lines.*

Figure 2(b): *Microcrack tending to be attracted towards the cement line.*

Two different simulations were carried out. In Simulation 1 we used images taken from transverse sections of cortical bone. The measured osteonal density (mean ± SD = 19.6 ± 1.4/mm2) was found to be within normal measured values [26]. Grids of straight lines were placed over the images, the points of intersection with cement lines were marked and their separations recorded. Some workers have noted that cracks which pass close to osteons tend to be attracted towards the cement line: one explanation for this is that the osteon is less well mineralised and so acts, to some extent, like a hole in the material, creating a local stress concentration [27]. To simulate this effect, we judged a crack tip to have reached a cement line if it passed within a length between the cement line and the average osteonal radiae length (60 μm). These measurements are illustrated in figure 3, in which the numbers represent the lengths between the osteons. Ten pictures from datasets 5, 6, 8 and 9 (bovine bones under 70 MPa) were selected for the osteonal density measurements, from which one of these was selected for Simulation 1 measurements under the mentioned density range.

Figure 3(a): *Vertical separations between cement lines are illustrated within the sections of cortical bone. Grid spaces are separated by 40*μm.

Figure 3(b): *Horizontal separations in a higher magnification, in order to display measurements between osteons. Grid spaces are separated by 40*μm. *Numbers represent lengths between osteons (*μm).

In Simulation 2 we used the same approach but instead of applying it to images of actual bone sections we used computer-generated images in which the osteons were represented by circles, placed at random locations, with diameters varying randomly between 100 and 300μm. We chose the same osteon density as measured experimentally, 19.5/mm^2, and the

same method of determining the lengths of simulated microcracks. Twenty models were generated with the use of the simulation program, performing an average of a_0 and α values, to be reported for the result of Simulation 2. Figure 4 displays an example of one simulation, with the inclusion of the simulated osteons.

Figure 4: *Conformation of simulated osteons in Simulation 2.*

Data Analysis and Statistics

For each case of experimental or simulated data, the results were plotted in terms of the cumulative probability as a function of crack length. The cumulative probability, which varies from 0 to 1, is the probability that a crack will be equal to or less than the specified length. For each set of data, theoretical curves were fitted assuming either a Weibull distribution or a Gaussian distribution.

For the two-parameter Weibull distribution, the relationship between cumulative probability P and crack length *a* is:

$$P = 1 - e^{-\left(a/a_0\right)^{\alpha}} \tag{1}$$

Here a_0 and α are constants.

In the case of a Gaussian distribution, the cumulative distribution function *F(a)* of crack length *a* is expressed as:

$$F(a) = P\left(\frac{a-\mu}{\sigma}\right) = \frac{1}{2\pi}\int_{-\infty}^{(a-\mu)/\sigma} e^{-u^2/2}du \tag{2}$$

Here *P* is the Cumulative Probability assuming a normal distribution; μ is the mean value and σ the standard deviation.

The accuracy (i.e. "Goodness of Fit") between the data and these two distributions was assessed using the Anderson-Darling (AD) approach [28]. The AD parameter has a different functional form depending on the distribution [29]. For a Gaussian distribution the form is:

$$AD = \sum_{i=1}^{n}\frac{1-2i}{n}\left\{\ln\left[P\left(\frac{a_i-\mu}{\sigma}\right)\right] + \ln\left[1-P\left(\frac{a_{n+1-i}-\mu}{\sigma}\right)\right]\right\} - n \tag{3}$$

For the Weibull distribution the form is:

$$AD = \left\{\sum_{i=1}^{n}\frac{1-2i}{n}\left\{\ln\left[1-\exp-\left(\frac{a_i}{a_0}\right)^{\alpha}\right] - \left(\frac{a_{n+1-i}}{a_0}\right)^{\alpha}\right\} - n\right\} \tag{4}$$

RESULTS

Figure 5 shows an example of the data analysis, in this case for data relating to the *in vivo* cracks found in bovine tibiae as reported in [16]. The data are plotted on two probability density plots, in one plot the axes are chosen such that the data should lie on a straight line if they conform to a normal (i.e. Gaussian) distribution, whilst in the other plot a straight line indicates the Weibull distribution. In this example the slightly lower AD value indicates that

the data are better described as a Weibull distribution. Table 2 shows AD values for all data examined; in all cases the Weibull distribution was found to be the better description.

Figure 5: *Example of dataset 5, showing cumulative probability P as a function of crack length a, on both Gaussian (i.e. Normal) and Weibull plots.*

Therefore a linear relationship on the plot is obtained by rearranging the equation as follows:

$$\ln\left[-\ln(1-P)\right] = \alpha\left[\ln a \ - \ln a_0\right] \qquad (5)$$

Thus by plotting the left hand side of this equation against ln *a* one obtains a straight line from which the two constants can easily be found. Fig.6 shows an example of this procedure for the case of our bovine bone *in vivo;* note that there is a slight discrepancy between the data and the line for the smallest crack lengths. The figure also shows the original P versus *a* plot with a line corresponding to the Weibull equation. When plotted in this form the error at low crack lengths is less evident: in fact it is a small absolute error which appears magnified owing to the logarithmic plot. The high R_2 value on the linear plot (0.97) is another indication of the accuracy of the fit. R_2 values for all datasets are presented in table 2.

Figure 6: *Example showing the original linear P/a plot (on the right) and its replotting to give a linear relationship (on the left) for the Weibull equation.*

Table 2: *Goodness of fit (Anderson-Darling parameter AD) between experimental crack length distributions and the Gaussian and Weibull predictions. Number of cracks and R_2 values of the Weibull distribution linearization are also shown.*

Table 3 shows the values of the two Weibull parameters for each dataset. Also shown in the table is the value of crack length which corresponds to a P value of 0.9, i.e. the length below which are found 90% of all cracks. This can be considered as a measure of the largest crack present, adjusted to remove effects of sample size. In what follows we will refer to this as a_{max}. In the current tests, 6 specimens didn't fracture, whereas 4 of them fractured with an average life of 159,700 cycles. Separation of the non-fractured and fractured specimens in table 3, shows no difference in α but a greater increase in a_o and a_{max} with number of cycles for the fractured specimens.

Table 3: *Weibull parameters for the various data sets, experimental and simulated. Data for the two studies on canine bone* in vivo *were combined, as were those for bovine bone.*

Figures 7-9 give a graphical display of the values of the three parameters, plotted as a function of number of cycles, N normalized by the number of cycles to failure N_f. The *in vivo* data are plotted at a value $N/N_f = 0$: for the canine data N_f was not known experimentally so it was estimated using methods established previously [30]. The α parameter is found to be relatively high for *in vivo* data and to fall with increasing number of cycles *in vitro*. The two *a* parameters show the opposite trend.

Figure 7: *The Weibull parameter α as a function of the normalised number of cycles to failure. Canine, ovine and bovine samples tested at different stress levels. In vivo data are shown at $N/N_f = 0$.*

Figure 8: *The Weibull parameter a_o as a function of the normalised number of cycles to failure. Canine, ovine and bovine samples tested at different stress levels. In vivo data are shown at $N/N_f = 0$.*

Figure 9: *The Weibull parameter a_{max} as a function of the normalised number of cycles to failure. Canine, ovine and bovine samples tested at different stress levels. In vivo data are shown at $N/N_f = 0$.*

Applying the t-test with a limit of p = 0.05 for statistically significant differences shows that for both canine and bovine bone the crack length distributions *in vivo* are different from those obtained by testing *in vitro*. Furthermore, for the bovine data, where we have test results at two different numbers of cycles, in both cases these also showed significant differences in crack length distributions. Significant differences were found for *in vivo* data from different species: ovine, canine and bovine. On the other hand, the two *in vivo* datasets of canine bone showed non-significant differences, as did the two sets of bovine *in vivo* data. In fact the high p values (0.65 for canine, 0.62 for bovine) suggest a reasonable degree of similarity for data obtained by different researchers at different times. So these datasets were pooled to increase sample size and facilitate comparison with other groups. There were non-significant differences between the bovine data at the same N value (50,000) at two different stresses (70MPa and 80MPa) and also non-significant differences between these two stresses when $N=N_f$.

DISCUSSION

This is the first time that an attempt has been made to describe the entire distribution of microcrack lengths in bone: previous studies have reported only the average length and the number density of cracks. There have been some other descriptions in the literature of crack length distributions in other materials (e.g. [31]) but overall this approach has not yet been developed to any significant extent. Knowledge of these distributions is potentially useful in understanding the mechanisms of crack growth and eventual failure and in developing theoretical models and simulations of material behaviour.

Here we showed that two-parameter Weibull distributions could accurately describe ten different sets of data from three different species, recording crack lengths *in vivo* and after cyclic testing *in vitro.* Of the two parameters, a_o is a kind of average crack length: strictly speaking it is the crack length which corresponds to a fixed value of the cumulative probability, of 0.63, so it is slightly larger than the median value; it will reflect, more or less, the mean values reported by other workers. The parameter α is a measure of the amount of scatter in the data: low values of α, as found here in all cases, indicate large variability in crack length, and the difference between the highest value, 4.1 and the lowest, 2 represents a very considerable change. High values of α imply that most cracks lie close to the median length, with few being very small, or, more importantly, very large.

We found a particularly high α value for *in vivo* ovine bone, but this may have more to do with the difference in bone type, as the rib was used here whilst all the other data relate to limb bones. Ribs experience a very large number of relatively constant loading cycles of breathing whilst the leg bones experience more variable cycling, with occasional high loadings due to running etc. It is also interesting to note that there are relatively large changes in the values of α and a_o for the in *vivo* data, but smaller differences in the value of a_{max}. In fact the three a_{max} values are all the same to within about 15%. This may be important because it is to be expected that the value of a_{max} will be the primary indicator of the risk of

failure. The number density of cracks in bone is relatively small, suggesting that failure occurs not by the accumulation and interaction of many small cracks, as it does in some other materials such as engineering fibre composites. Rather, the likely failure scenario for bone is that one crack grows to become large enough to cause failure on its own. Some support for this scenario comes from the a_{max} values for the bovine bone tested at two different stress levels, which are quite similar at $N=N_f$, and it is interesting that when we distinguished in our test data those samples that fractured from those that did not, the value of a_{max} was greater in the fractured group. For bone, control of a_{max} is the key to prevent failure, and this can be done efficiently by selectively removing the longer cracks. Selectively removing longer cracks implies that living bone is able to detect and measure crack lengths in order to choose the longest ones for repair. This question is one which is being actively investigated by various research groups (including the current group). Currently it has been established that bone is able to detect cracks and target them for repair, though whether it can distinguish between long and short cracks is not clear.

In vitro loading caused changes in the crack length distributions as reflected in the Weibull parameters (figs 7-9); crack lengths a_o and a_{max} increased, and α decreased. The increases in a_o and a_{max} are to be expected given that some of the cracks were growing during the tests. Differences were found even in the case of the canine data which were cycled at a strain level within the normal physiological range – in this case the major factor is presumably the lack of repair, implying that *in vivo* repair may be targeted towards the longer cracks. The decrease in α during cycling of both canine and bovine bone could have two possible explanations: new, small cracks could be initiating and/or some of the existing cracks could be elongating, whilst others do not.

As indicated in table 4, Weibull values calculated from the performance of simulations of simulated cracks being attracted only when reaching cement lines, as well as when passing within length ranges longer than the average lengths of osteonal radiae (60 μm) present inaccurate values compared to those in realistic failure conditions (*in vitro* datasets 9 and 10). Consideration for simulations of cracks attracted towards the osteons in a length range between the cement lines and the average lengths of osteonal radiae (approx. 40 μm), give considerably similar Weibull values compared to those of datasets 9 and 10 (table 3). This last result indicates that cracks tend to be attracted towards osteons when passing within a length between osteon cement lines and no further than the osteon radiae lengths. Our attempts to simulate crack distributions resulted in relatively large crack lengths (especially Simulation 1) and high scatter (especially Simulation 2) though the results were quite similar to the data from bones tested to failure *in vitro*. This suggests that a simple model of microcrack growth, in which cracks extend until they meet cement lines, is a reasonable description.

Knowledge of these distribution functions will facilitate the creation of theoretical models and computer simulations which attempt to reproduce the mechanical behaviour of bone. One interesting result seen in the bovine bone data is that whilst the parameters change significantly with number of cycles, they are not affected by stress level, at least for the stress levels used here. Of course the numbers of cracks present, and the number of cycles to failure, are both strong functions of stress, but it seems that the distribution of lengths remains the same; results published previously [32] help support this, where the authors conclude that mean crack densities in bone increase significantly with age, while mean lengths do not. This suggests that the distribution is largely controlled by the microscopic

structure of the bone, especially the spacing of secondary osteons and other barriers to crack growth such as the brick-like structures in plexiform bone.

As an example of the potential use of this approach in theoretical modeling, we consider the effect of the total number of cracks present. For a given number density, larger bones (and bones in larger animals) will have more cracks. For a given distribution (i.e. given values of α and a_o) this implies that the largest crack will be longer, and thus the bone will be more likely to fail. Consider a number of cracks, n, having a distribution according to the Weibull equation (equation (1)). The probability that all these cracks will be less than some length *a* is:

$$P = \left[1 - e^{-\left(\frac{a}{a_o}\right)^{\alpha}} \right]^n \qquad (6)$$

If we set this probability to 0.5 and rearrange the equation we can find the average length of the longest crack, a_{avmax}

$$a_{avmax} = a_o(-\ln(1-0.5^{1/n}))^{1/\alpha} \qquad (7)$$

Figure 10 shows the function graphically using the parameters found for canine bone *in vivo*.

Figure 10: *Relationship between a_{max} and bone size, represented by the total number of cracks, n, using the data from in vivo canine bone.*

This shows a large increase in the lengths of the longer cracks when there are more cracks present. Given that the stresses and strains in bones seem to be approximately constant over animals of different sizes [19], larger animals would need to compensate for this effect if their bones are to be as strong as those of smaller animals. This might be done, for example, by reducing the number density of cracks in large bones, or by increasing osteon density to reduce the distance between cement lines. This analysis thus suggests an avenue for future experimental work. There is already evidence for this compensation effect in some of our previous work [30] which showed that, when considering test specimens of equal size, bone from larger animals has higher fatigue strength than bone from smaller animals.

CONCLUSIONS

- Microcracks which naturally occur in bone *in vivo* have a distribution of lengths which can be accurately described by the two-parameter Weibull equation.
- Cyclic loading applied to bones *in vitro* alters this distribution; it can still be described by the Weibull equation, but with different parameters.
- The values of the Weibull parameters differ according to bone type/species, and vary in a systematic way with number of cycles during *in vitro* testing. They do not appear to be affected by applied stress level, at least for the limited range of stresses investigated.
- The description of microcrack populations using this approach provides new information which can be useful in discussing the mechanisms of microdamage, repair and failure.

- The more cracks are present, the more long cracks grow, so crack accumulation leads to failure.

ACKNOWLEDGEMENTS

We are grateful to the following authors for generously providing us with their original data:

- Prof. David Burr; Department of Anatomy, Indiana University School of Medicine, Indianapolis, IN 46202, U.S.A.
- Prof. Peter Muir; Comparative Orthopaedic Research Laboratory, Department of Surgical Sciences, School of Veterinary Medicine, University of Wisconsin-Madison, Madison, WI, U.S.A.
- Dr. Mohammed Faraz Khan; Department of Anatomy, Royal College of Surgeons in Ireland.

Funding for this work was provided by the Department of Education and Science, Government of Ireland, and the National Council on Science and Technology of Mexico.

REFERENCES

1. J. Bloomfield, P.A. Fricker, and K.D. Fitch, Science and Medicine in Sport, 2nd ed., Blackwell Science, Oxford, 1995
2. G.N. Guten, Running Injuries, W.B. Saunders Company, Philadelphia, 1997.
3. A.J. Campbell, M.C. Robertson, and M.M. Gardener, Falls prevention over 2 years: a randomised control trial in women 80 years and older, Age Ageing, 28 (1999) 513-518.
4. J.D. Currey, Bones, P.U. Press, Woodstock, Oxfordshire, 2002.
5. R.B. Martin, D.B. Burr, Skeletal Tissue Mechanics, S.-. Verlag, New York, 1998.
6. H.M. Frost, Preparation of thin undecalcified bone sections by rapid manual method. Stain Technol, 33 (1958) 273-277.
7. H.M. Frost, Presence of microscopic cracks in vivo in bone, Henry Ford Hosp Med Bull, 8 (1960) 25–35.
8. N.L. Fazzalari, Assessment of Cancellous Bone Quality in Severe Osteoarthrosis: Bone Mineral Density, Mechanics, and Microdamage, Bone, 22(4) (1998) 381-388.
9. J.D. Frank, Aging and accumulation of microdamage in canine bone, Bone, 30(1) (2002) 201-206.
10. P. Muir, K.A. Johnson, C.P. Ruaux - Mason, In Vivo Matrix Microdamage in a Naturally Occurring Canine Fatigue Fracture, Bone, 25(5) (1999) 571–576.
11. T.L. Norman, Z. Wang, Microdamage of human cortical bone: Incidence and morphology in long bones, Bone, 20(4) (1997) 375-379.
12. O. Akkus, C.M. Rimnac, Cortical bone tissue resists fatigue fracture by deceleration and arrest of microcrack growth, J Biomech, 34(6) (2001) 757-764.
13. J.J. Kruzic, R.O. Ritchie, Fatigue of Mineralized Tissues: Cortical Bone and Dentin. J Mech Behav Biomed Mater, 1 (2008) 3-17.
14. D. Taylor, T.C. Lee, Microdamage and mechanical behaviour: predicting failure and remodelling in compact bone, J Anat, 203(2) 2003 203-211.
15. M.F. Khan, Microdamage and remodelling in an ovine model, NUI, Royal College of Surgeons in Ireland, 2010.
16. F.J. O' Brien, D. Taylor, T.C. Lee, Microcrack accumulation at different intervals during fatigue testing of compact bone, J Biomech, 36(7) (2003) 973-980.
17. D.B. Burr, Does microdamage accumulation affect the mechanical properties of bone?, J Biomech, 31(4) (1998) 337-345.
18. K.L. Gellasch, V.L. Kalscheur, Fatigue microdamage in the radial predilection site for osteosarcoma in dogs, Am J Vet Res, 63(6) (2002) 896-899.

19. C.T. Rubin, L.E. Lanyon, Regulation of bone mass by mechanical strain magnitude, Calcif Tissue Int, 37 (1985) 411–417.
20. D.B. Burr, C. Milgrom, In vivo measurement of human tibial strains during vigorous activity, Bone, 18(5) (1996) 405-410.
21. D.M. Nunamaker, D.M. Butterweck, M.T. Provost, Fatigue fractures in thoroughbred racehorses: Relationships with age, peak bone strain, and training, J Orthop Res, 8 (1990) 604-611.
22. L.V. Griffin, J.C. Gibeling, Model of flexural fatigue damage accumulation for cortical bone, J Orthop Res, 15(4) (1997) 607-614
23. F.J. O' Brien, Behaviour of Microcracks in Compact Bone, Eur J Morphol, 42(1/2) (2005) 71-79.
24. F.J. O' Brien, D. Taylor, T.C. Lee, Bone as a composite material: The role of osteons as barriers to crack growth in compact bone, Int J Fatigue, 29(6) (2007) 1051-1056.
25. M.B. Schaffler, K. Choi, C. Milgrom, Aging and matrix microdamage accumulation in human compact bone, Bone, 17(6) (1995) 521-525.
26. S. Mohsin, F.J. O'Brien, T.C. Lee, Osteonal crack barriers in ovine compact bone, J Anat, 208 (2006) 81–9.
27. O.D. Kennedy, The effects of increased intracortical remodeling on microcrack behaviour in compact bone, Bone, 43 (2008) 889–893.
28. NIST, Engineering Statistics Handbook, National Institute of Standards and Technology, NIST/SEMATECH e-Handbook of Statistical Methods, http://www.itl.nist.gov/div898/handbook/. p. 1.4.2.9.2., 2003.
29. J.L. Romeu, Anderson-Darling: A Goodness of Fit Test for Small Samples Assumptions, Selected Topics in Assurance Related Technologies (START), 10(5) (2003) 1-6.
30. D. Taylor, Scaling Effects in the Fatigue Strength of Bones from Different Animals J Theor Biol, 206(2) (2000) 299-306.
31. L.R. Botvina, Damage Evolution on Different Scales, in 17th European Conference on Fracture, Institute of Metallurgy and Materials Science, Russian Academy of Sciences: Brno, Czech Republic, 2008.
32. N. Wasserman, B. Brydges, S. Searles, O. Akkus, In vivo linear microcracks of human femoral cortical bone remain parallel to osteons during aging, Bone, 43(5) (2008) 856-861.

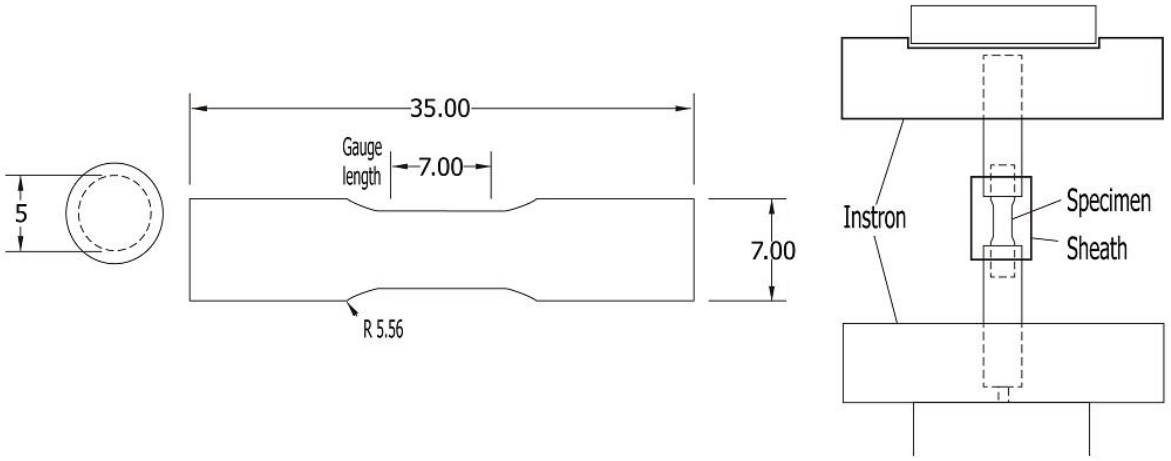

Figure 1: *Details of specimens and their orientation in the testing machine. All dimensions in millimetres.*

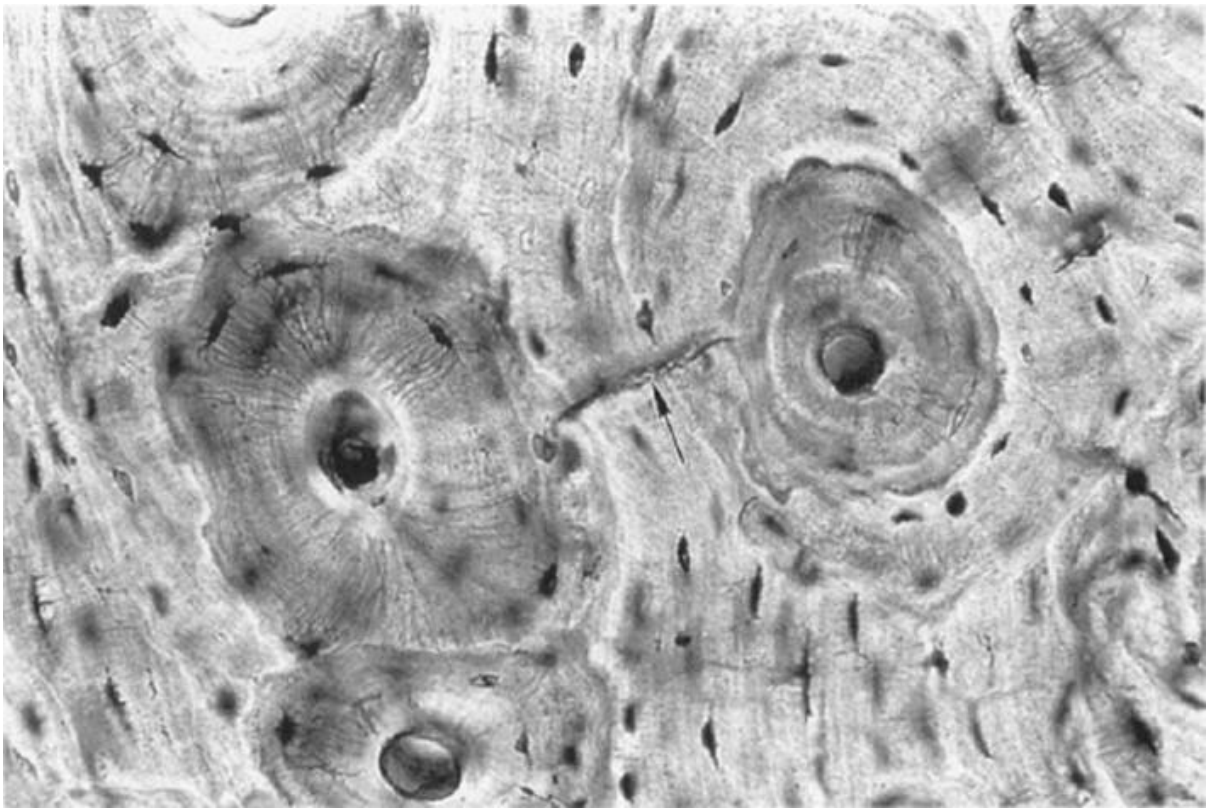

Figure 2(a): *Microcrack growth stopped by its tips when encountering the cement lines.*

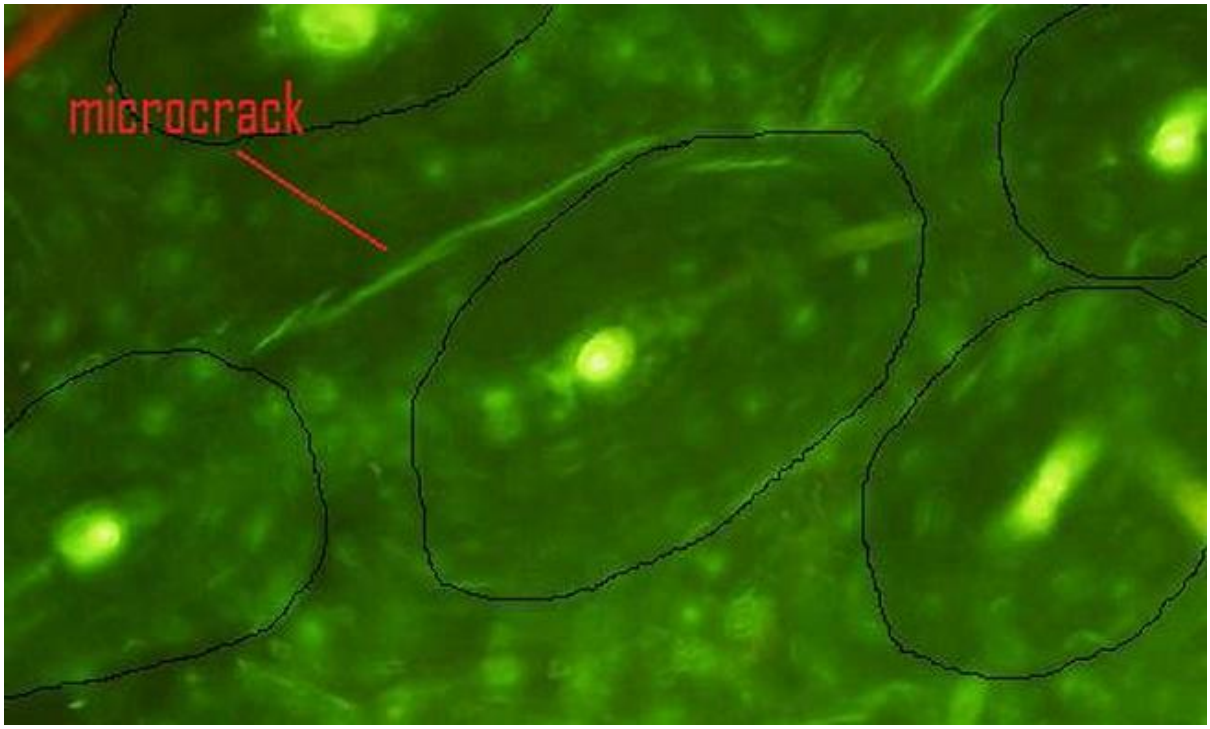

Figure 2(b): *Microcrack tending to be attracted towards the cement line.*

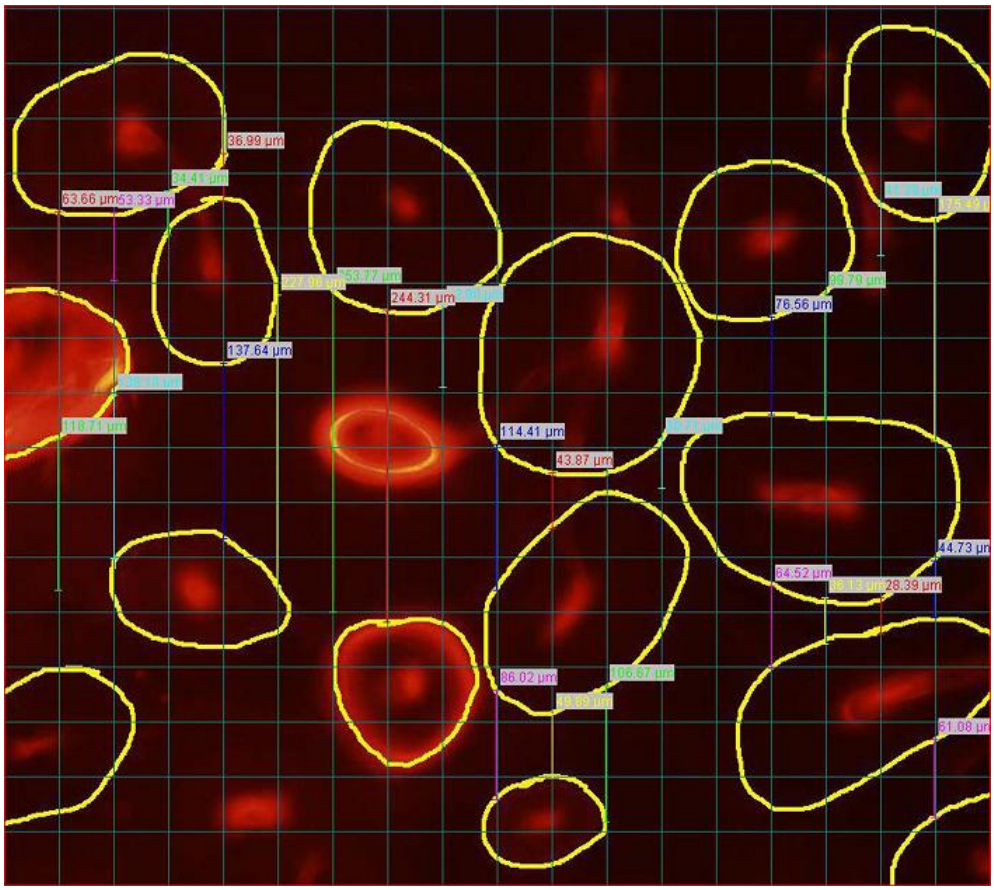

Figure 3(a): *Vertical separations between cement lines are illustrated within the sections of cortical bone. Grid spaces are separated by 40µm.*

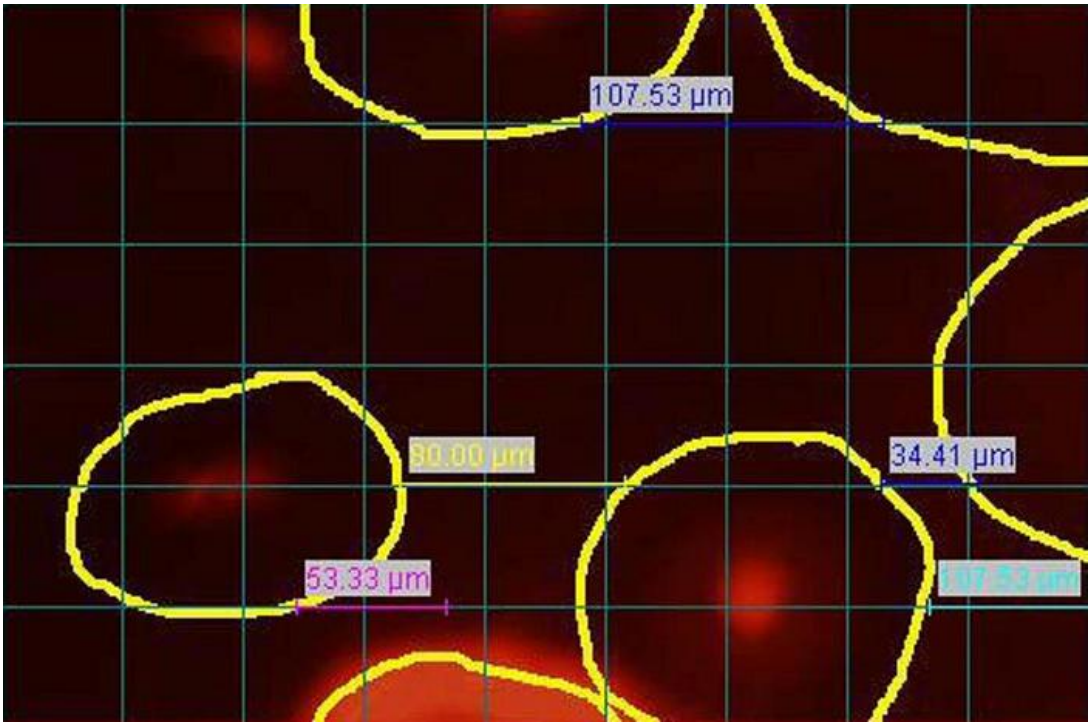

Figure 3(b): *Horizontal separations in a higher magnification, in order to display measurements between osteons. Grid spaces are separated by 40 µm. Numbers represent lengths between osteons (µm).*

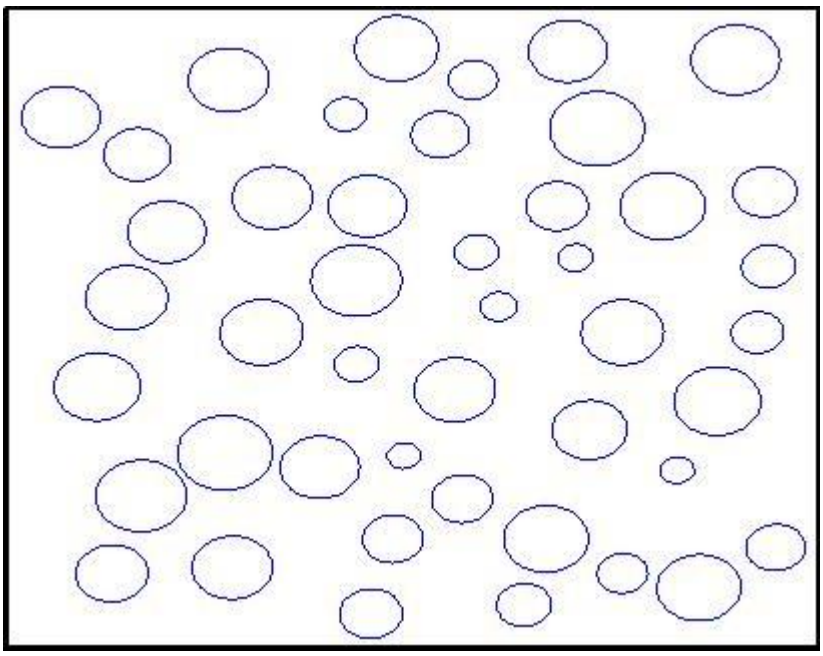

Figure 4: *Conformation of simulated osteons in Simulation 2.*

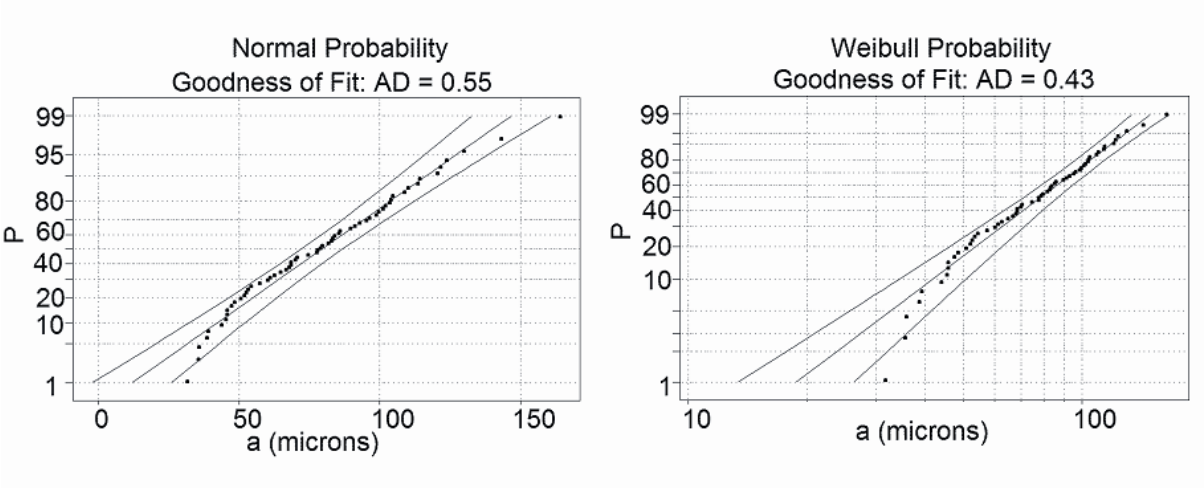

Figure 5: *Example of dataset 5, showing cumulative probability P as a function of crack length a, on both Gaussian (i.e. Normal) and Weibull plots.*

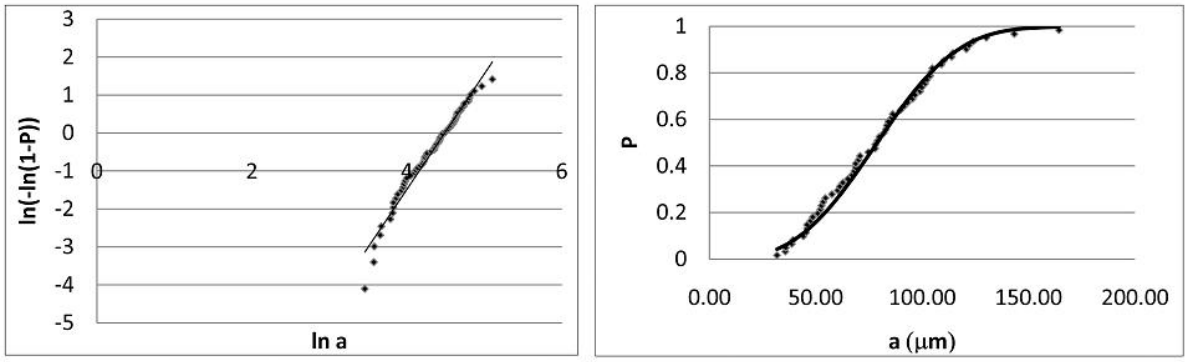

Figure 6: *Example showing the original linear P/a plot (on the right) and its replotting to give a linear relationship (on the left) for the Weibull equation.*

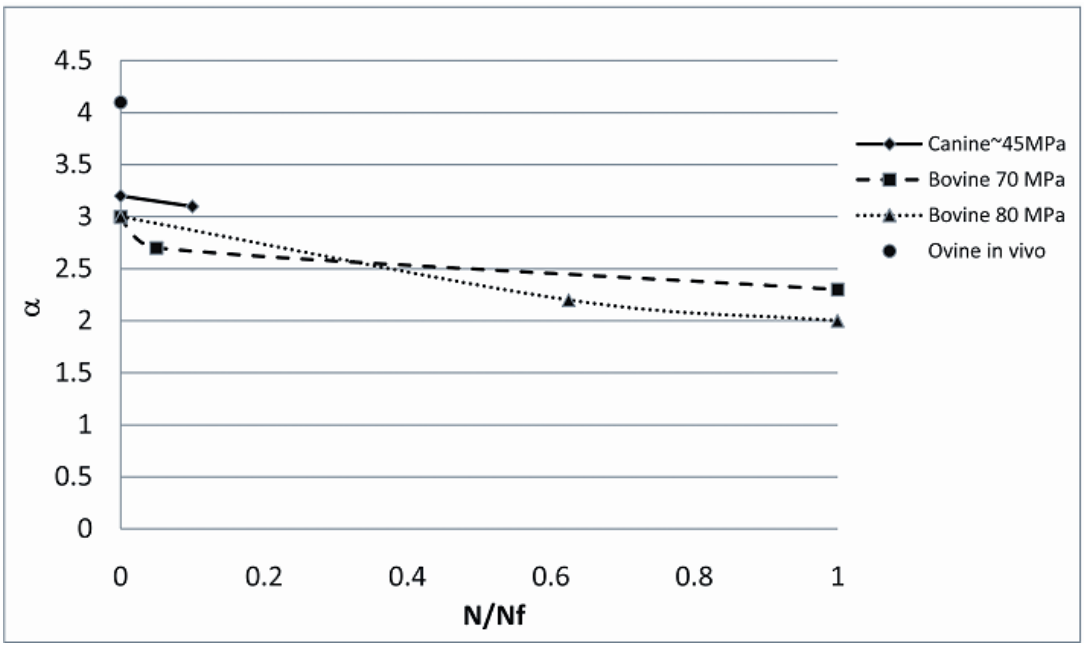

Figure 7: *The Weibull parameter α as a function of the normalised number of cycles to failure. Canine, ovine and bovine samples tested at different stress levels. In vivo data are shown at $N/N_f = 0$.*

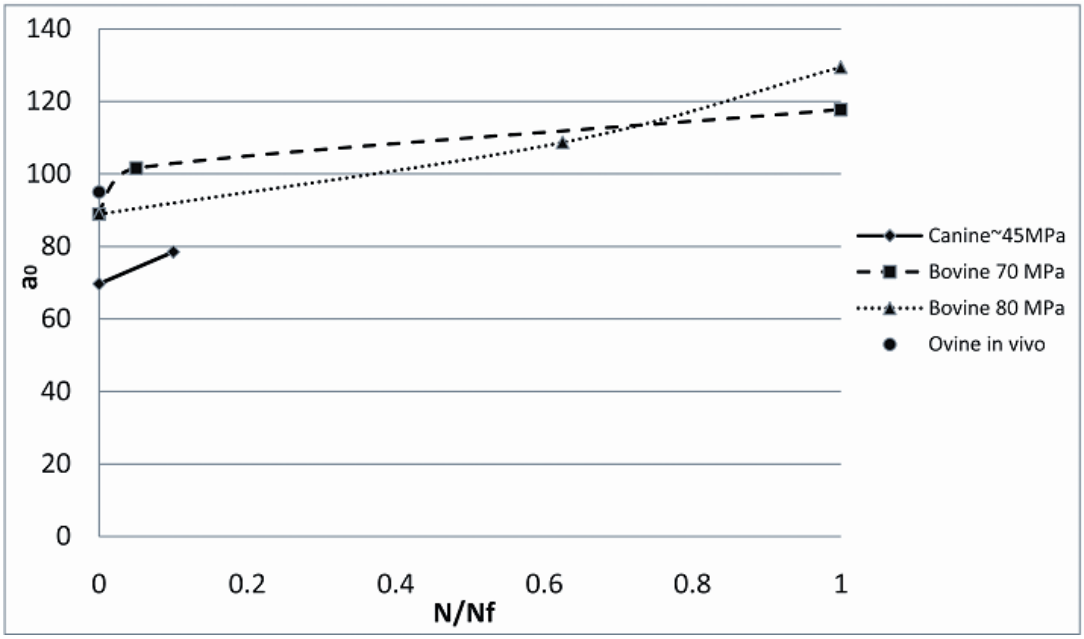

Figure 8: *The Weibull parameter a_o as a function of the normalised number of cycles to failure. Canine, ovine and bovine samples tested at different stress levels. In vivo data are shown at $N/N_f = 0$.*

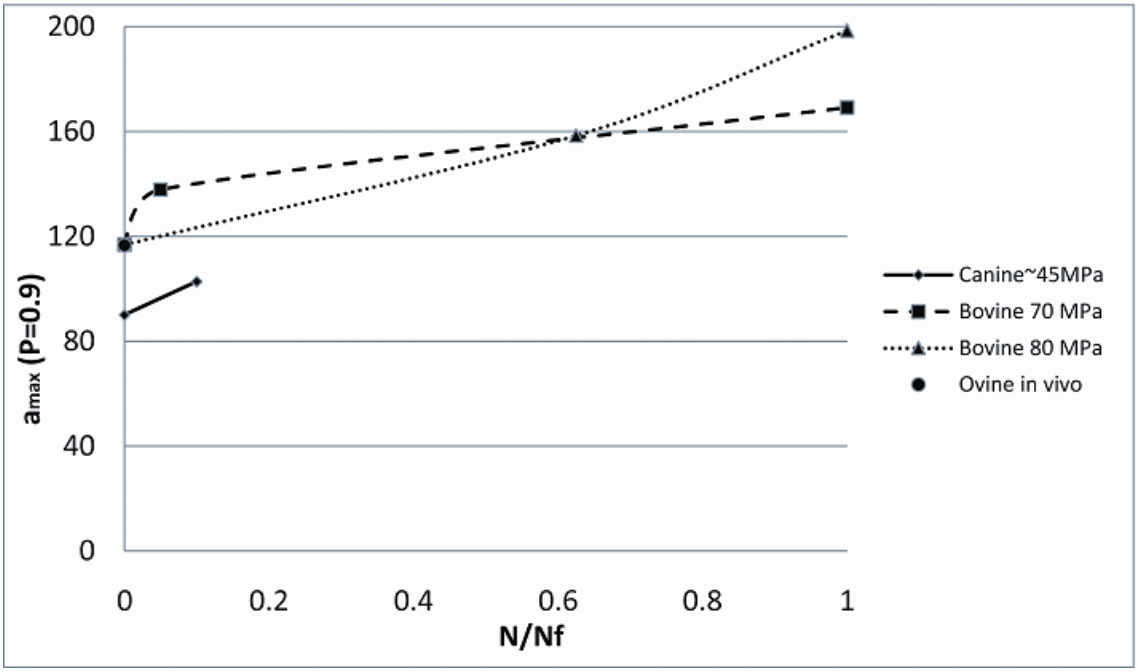

Figure 9: *The Weibull parameter a_{max} as a function of the normalised number of cycles to failure. Canine, ovine and bovine samples tested at different stress levels. In vivo data are shown at $N/N_f = 0$.*

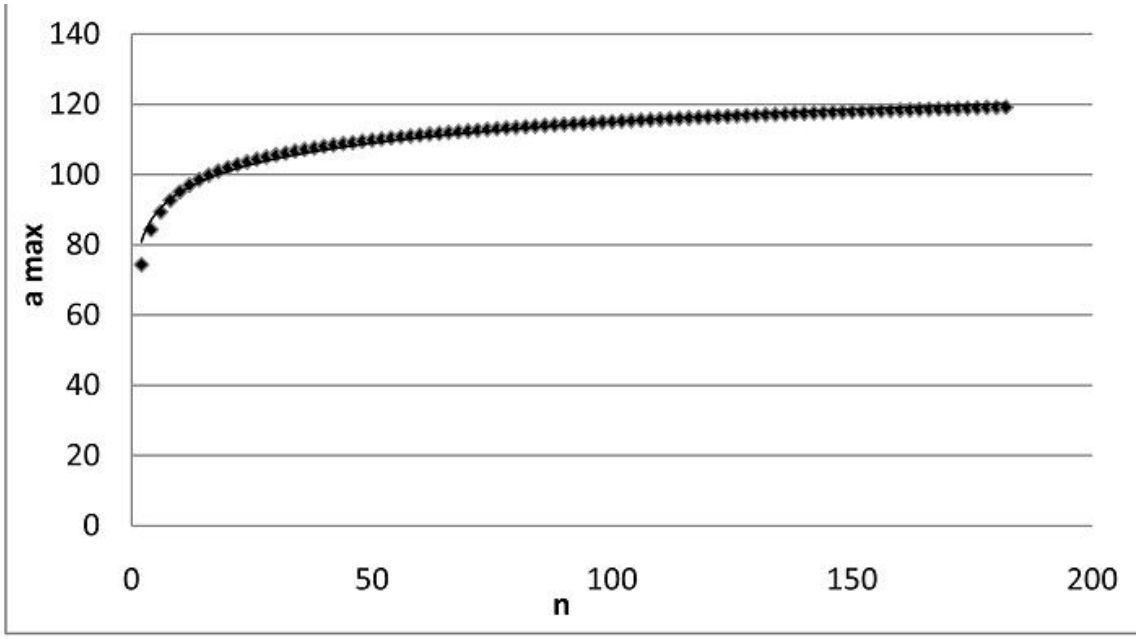

Figure 10: *Relationship between a_{max} and bone size, represented by the total number of cracks, n, using the data from in vivo canine bone.*

Dataset	Bone type	Stress	Number of cycles	Reference
1	Canine radius	In vivo	In vivo	[18]
2	Canine femur	In vivo	In vivo	[17]
3	Canine femur	2700 με	approx. 426000 cycles	[17]
4	Ovine rib	In vivo	In vivo	[15]
5	Bovine tibia	In vivo	In vivo	[16]; Present study
6	Bovine tibia	70 MPa	50000 cycles	Present Study
7	Bovine tibia	80 MPa	50000 cycles	[16]
8	Bovine tibia	70 MPa	Million cycles non fractured	Present Study
9	Bovine tibia	70 MPa	Fracture av. 159700 cycles	Present Study
10	Bovine tibia	80 MPa	Fracture av. 88000 cycles	[16]

Table 1

Dataset	AD Gaussian	AD Weibull	Number of cracks	R^2 linear plot
1	15.05	13.44	672	0.92
2	0.74	0.71	25	0.97
3	1.28	0.98	96	0.94
4	0.72	0.69	34	0.95
5	0.55	0.43	60	0.97
6	3.22	1.8	120	0.95
7	4.88	3.45	48	0.78
8	14.91	8.97	190	0.84
9	3.01	1.75	84	0.93
10	4.53	1.92	95	0.91

Table 2

Dataset	α	a_0 (μm)	a_{max} (μm) (P=0.9)
1, 2	3.2	69.7	90.1
3	3.1	78.5	102.8
4	4.1	95.0	116.7
5	3.0	88.9	116.9
6	2.4	113.1	159.9
7	2.2	108.7	158.5
8	2.3	113.8	163.5
9	2.3	126.0	181.1
10	2.0	129.4	198.5
Simulation 1	1.9	131.3	203.6
Simulation 2	1.4	113.1	205.2

Table 3

	α	a_0 (μm)	a_{max} (μm) (P=0.9)
Simulation. No length consideration; direct contact with osteonal cement lines.	1.6	174.6	294.1
Simulation. Range between cement lines and average lengths of osteonal radiae (40 μm).	1.9	131.3	203.6
Simulation. Range higher than average lengths of osteonal radiae (60 μm)	2.2	115.21	168.3
Simulation. Range higher than average lengths of osteonal diameters (120 μm)	2.8	92.93	125.2
Experimental tests. Dataset 9	2.3	126.0	181.1
Experimental tests. Dataset 10	2.0	129.4	198.5

Table 4: *Weibull values of differing length ranges for cracks to be attracted towards osteons.*